

Physical Optics Analysis for RCS Computation of a Relatively Small Complex Structure

Amin B. Gorji ¹, Bijan Zakeri ¹, and Reza C. Janalizadeh ²

¹ Faculty of Electrical and Computer Engineering
Babol Noshirvani University of Technology, Babol, Iran
amin.gorji@stu.nit.ac.ir, zakeri@nit.ac.ir

² School of Electrical and Computer Engineering
University of Tehran, Tehran, Iran
r.janalizadeh@ut.ac.ir

Abstract — High-frequency methods are well known as a convenient approach for treating Electromagnetic (EM) problems regarding electrically large structures. In this paper however, this method is proposed as a proper tool for computing the mono-static Radar Cross Section (RCS) of a relatively small complex structure. This claim has been verified via simulation through a frequency range of 100 MHz to 10 GHz and measurement for the structure of this work. In this regard, initially, RCS computation via the Method of Moments (MoM) has been executed. As this method leads to rigorous and time consuming computations, Physical Optics (PO) has been utilized for the same purpose. These computations have been carried out by employing the Integral Equation (IE) and asymptotic solver of CST Microwave Studio (MWS). PO proves to be time-efficient compared to MoM. Graphs comparing PO and MoM-computed RCS are illustrated. In addition, the similarity of the results obtained by PO and MoM has been thoroughly discussed. Correlation between these results has been observed. Also, mean and standard deviation values for PO RCS-error have been provided for the entire simulation frequency. As dimension to wavelength ratio (D/λ) of the structure increases, the convergence of these two methods for RCS computation becomes satisfactory. Finally, measurement has been accomplished at frequency of 8.5 GHz to validate PO computations.

Index Terms — Complex structure, Integral

Equation (IE), Method of Moments (MoM), Physical Optics (PO) and Radar Cross Section (RCS).

I. INTRODUCTION

Target detection has been of great interest in both civilian and military applications [1]-[17]; e.g., through wall imaging during rescue operations in disastrous areas, identification of objects buried under rough surface, ships floating over the sea surface and targets inside vegetation. Characterization of Electromagnetic (EM) wave propagation and scattering from targets provides data for Radar Cross Section (RCS) prediction and Synthetic Aperture Radar (SAR) image construction of corresponding targets [18]-[20].

RCS computation and scattering analysis of electrically large targets located in natural environment via the Method of Moments (MoM), have been under study for many years. However, complexities due to large target size and multi-interactions between the target and surrounding media, make the simulation process much more rigorous; especially in high frequencies. However, high frequency methods such as Geometrical Optics (GO), Physical Optics (PO), Geometrical Theory of Diffraction (GTD), Physical Theory of Diffraction (PTD), Shooting and Bouncing Rays (SBR), etc., have been applied to the EM scattering of these structures with good accuracy and convincing physical insight [21]-[25]. Meanwhile, the RCS of electrically small simple targets located above rough surfaces has been computed accurately

via GO, PO and Iterative Physical Optics (IPO) [26]-[27].

A complex structure consists of several reflectors within a radar resolution cell. According to this definition, almost all real world maritime targets are complex structures. For such targets, there is no analytical relationship between the target's surface and its RCS.

In this paper, the RCS of a relatively small *complex* structure have been computed via PO and MoM. Then the similarity of RCS results have been assessed. A minimum dimension to wavelength ratio (D/λ), resulting in precise RCS computation by means of PO, is then obtained. The rest of the paper is organized as follows: In section II, a relatively small model of a vessel has been introduced as the complex structure. The geometry of the problem and simulation frequency range is included in this section. In section III, the methods by which RCS computation has been performed are introduced. The IE and asymptotic solver of the commercial software CST Microwave Studio (MWS) have been employed for this purpose. Resulted RCS plots, error tables and correlation graphs for three view angles: azimuth, elevation along the length and elevation along the width are provided and analyzed through the frequency range of 100 MHz to 10 GHz in section IV. A minimum D/λ for an accurate RCS computation by means of PO is investigated in this section. Finally, in section V, measurement has been accomplished at 8.5 GHz for azimuth view in order to validate PO for the RCS computation of the vessel.

II. STRUCTURE PROFILE & SIMULATION SETUP

A. Model description

The complex structure selected for RCS computation is the scaled model of a typical vessel depicted in Fig. 1. Also, Table 1 provides dimensions for the same structure.

B. Geometry of the problem

The simulation has been performed for three different view aspects: azimuth, elevation along the length of the vessel and elevation along the width of the vessel. As depicted in Fig. 1 (a), azimuth view aspect is demonstrated by sweeping φ from 0 to 2π , elevation along the length view is acquired while sweeping θ from 0 to π , as shown in Fig. 1 (b)

and elevation along the width view is attained while sweeping θ from 0 to π , as in Fig. 1 (c); in which θ and φ are elevation and azimuth angles, respectively.

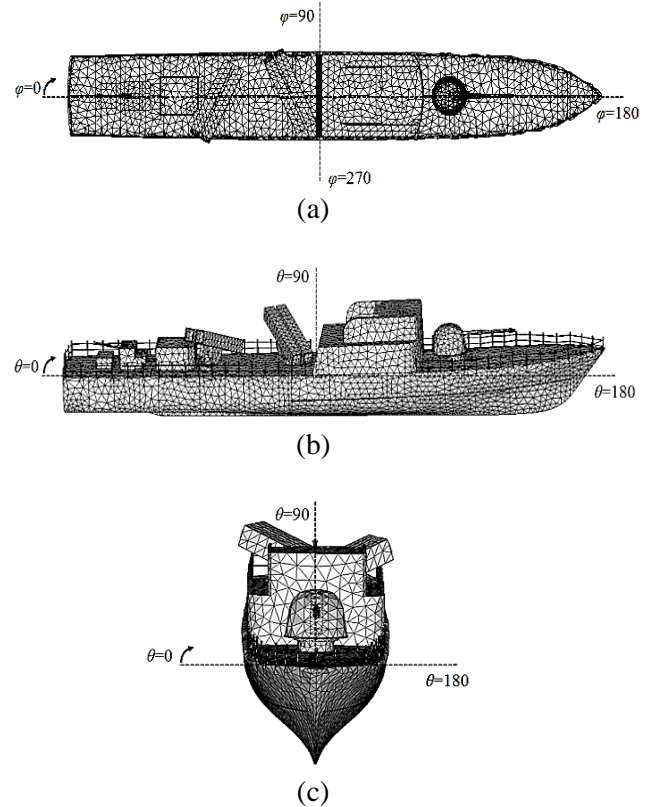


Fig. 1. View aspects for the meshed vessel: (a) azimuth, (b) elevation along the length and (c) elevation along the width.

Table 1: Dimensions of the structure

Width	Length	Height
8.25 cm	58.75 cm	6.27 cm

C. Frequency range

PO approximation gives convenient and simple expressions for the scattering cross section and therefore is widely used. This approximation contains wavelength dependence and the results are often in good agreement with experimental data, even though it is difficult to establish exactly how valid PO is for a general case [28].

Previous numerical studies using MoM and FDTD have given broad assessments of the reliability of PO. For instance, the validity and accuracy study of PO method for the reduced-size

lens antennas and rough surface scattering models [26]-[27], [29]. In the former study, it has been shown that PO can be used for analyzing lens antennas typically larger than 5λ , where λ is the wavelength. In [27], quite acceptable results have been shown using GO and PO for the RCS prediction of a PEC target with dimensions $4\lambda/3 \times 2\lambda/3 \times \lambda$ above a Gaussian random rough surface, with $Z_s = Z_0(0.2 + j0.02)$, rms height of 5 cm and correlation length of 40 cm at 2 GHz frequency. Also, the RCS of an object with surface impedance $Z_s = Z_0(0.2 + j0.02)$ and dimensions less than 8λ and more than 1.5λ has been precisely computed in the same frequency in the same work.

In this work, the central simulation frequency is chosen in a manner which the corresponding minimum D/λ determined by the height (smallest dimension) of the structure is identical to the lower limits of D/λ (approximately 1) in works mentioned previously [26], [27]. In this case, RCS precision is analyzed in the vicinity of a frequency, which PO RCS computation of prototype objects is performed with an adequate accuracy.

III. METHODS OF ANALYSIS

A. Physical optics

It is common practice in the analysis of EM boundary-value problems to use auxiliary vector potentials \vec{A} and \vec{F} as aids in obtaining solutions for the electric \vec{E} and magnetic \vec{H} fields. The vector potentials are given by:

$$\vec{A} = \frac{\mu_0}{4\pi} \int_V \vec{J}(\vec{r}') \frac{e^{-jk|\vec{r}-\vec{r}'|}}{|\vec{r}-\vec{r}'|} dv', \quad (1)$$

and

$$\vec{F} = \frac{\epsilon_0}{4\pi} \int_V \vec{M}(\vec{r}') \frac{e^{-jk|\vec{r}-\vec{r}'|}}{|\vec{r}-\vec{r}'|} dv', \quad (2)$$

where \vec{J} and \vec{M} are electric and magnetic current sources, respectively and k is the wavenumber.

PO is a method for approximating high frequency surface currents. If the object is large compared to a wavelength and the surface is smooth (radius of curvature is much greater than a wavelength), \vec{J} may be well approximated by the current that would exist if the surface were a conducting plane tangential to the surface at the point \vec{r}' . In this case $\vec{J}_s = 2\hat{n} \times \vec{H}^i$ in the region illuminated by the incident field, while $\vec{M}_s = 0$.

Subscript s demonstrates the surface nature of the current source and \hat{n} is the unit vector normal to the surface. The $\hat{i} \cdot \hat{n} < 0$ holds for the region illuminated by the incident field, where \hat{i} is a unit vector in the direction of incidence. Assuming $(\nabla \cdot \vec{A}) = 0$, the EM fields are:

$$\vec{E} = -j\omega\vec{A}, \quad (3)$$

and

$$\vec{H} = \frac{1}{\mu_0} \nabla \times \vec{A}. \quad (4)$$

Suppose the structure depicted in Fig. 1 is illuminated by an incident plane wave as:

$$\vec{E}^i(\vec{r}) = E^i e^{-jk(\hat{i} \cdot \vec{r})} \hat{e}^i. \quad (5)$$

The surface current will be:

$$\vec{J}_s(\vec{r}') = \frac{2}{\eta_0} E^i e^{-jk(\hat{i} \cdot \vec{r}')} \hat{n} \times (\hat{i} \times \hat{e}^i), \quad (6)$$

where

$$\vec{H}^i = \frac{1}{\eta_0} (\hat{i} \times \vec{E}^i), \quad (7)$$

has been used for the relation between the incident plane wave magnetic and electric fields and $\eta_0 = 120\pi$ ohm is the free space characteristic impedance. The far-field magnetic vector potential is well known as:

$$\vec{A}_{ff} = \frac{\mu_0}{4\pi} \frac{e^{-jk|\vec{r}|}}{|\vec{r}|} \int_V \vec{J}(\vec{r}') e^{jk(\vec{r}' \cdot \hat{r})} dv'. \quad (8)$$

Therefore, the far-field scattered electric field will be:

$$\vec{E}_{ff}^s = -jk \frac{e^{-jk|\vec{r}|}}{2\pi |\vec{r}|} E^i \int_S (\hat{i}(\hat{n} \cdot \hat{e}^i) - \hat{e}^i(\hat{n} \cdot \hat{i})) e^{-j2k(\hat{i} \cdot \vec{r}')} ds', \quad (9)$$

where the BAC-CAB identity has been used for the cross product $\hat{n} \times (\hat{i} \times \hat{e}^i)$. As is usually the case, the antenna receives the component of the scattered wave along the direction of the polarization of the incident wave \hat{e}^i . Thus, the far-field scattered electric field received by the antenna will be:

$$\begin{aligned} \vec{E}_r^s &= (\vec{E}_{ff}^s \cdot \hat{e}^i) \hat{e}^i \\ &= jk \frac{e^{-jk|\vec{r}|}}{2\pi |\vec{r}|} E^i \int_S (\hat{n} \cdot \hat{i}) e^{-j2k(\hat{i} \cdot \vec{r}')} ds' \hat{e}^i. \end{aligned} \quad (10)$$

Regarding the definition of RCS as:

$$\sigma = \lim_{|\vec{r}| \rightarrow \infty} 4\pi |\vec{r}|^2 \frac{|\vec{E}_r^s|^2}{|\vec{E}^i|^2}, \quad (11)$$

we get:

$$\sigma = \frac{k^2}{\pi} \left| \int_S (\hat{n} \cdot \hat{i}) e^{-j2k(\hat{i} \cdot \vec{r}')} ds' \right|^2, \quad (12)$$

for the scattering cross section of a conducting body. While robust, PO does not account for the fields diffracted by edges or those from multiple reflections, so supplemental corrections are usually added to it. The PO method is used extensively in high-frequency reflector antenna analysis, as well as radar cross section prediction [30], [31].

The asymptotic solver of CST MWS is based on the SBR method and accounts for the multiple scattering effect [32]. It computes PO scattered fields too. As the effect of the sea rough surface and the vessel structure itself on multiple scattering has been neglected, only RCS calculations via PO have been done.

The SBR method was developed to predict the multiple-bounce backscatter from complex objects. It uses the ray optics model to determine the path and amplitude of a ray bundle, but uses a PO based scheme that integrates surface currents deposited by the ray at each bounce point. The SBR method is used in RCS prediction of cavities [25] and image formation of targets [33]. Also, it is used to predict wave propagation and scattering in complex urban environments to determine the coverage for cellular telephone service [34].

B. Method of moments

CST MWS incorporates an integral equation solver [32]. This solver employs a MoM discretization with a surface integral formulation of the electric and magnetic field. In other words, the discretization of the calculation area is reduced to the object boundaries; thus, leading to a linear equation system with fewer unknowns than volume methods. In order to reduce the numerical complexity, a Multilevel Fast Multipole Method (MLFMM) approach has been used.

IV. RESULTS AND DISCUSSION

RCS computation and scattering analysis of electrically large targets via MoM, possesses complexities which result in rigorous simulation

processes; especially in high frequencies. This issue has also been confronted during the RCS computation of the vessel. PO has been employed in order to solve this complication.

Referring to [26], [27], it is seen that PO provides precise results for the RCS of simple objects with a minimum D/λ of 1. During this work, the same D/λ has been chosen to assess the accuracy of PO RCS computations. As for the vessel, this minimum has been used to acquire the central value of the simulation frequency. As in a constant frequency, the height of the vessel results in the minimum D/λ , a value of 1 for this parameter is analogous to a simulation frequency of 5 GHz. However, in order to thoroughly analyze the reliability of PO, a symmetric 10 GHz frequency range has been set providing results for D/λ 's much less than those cited in [26], [27].

Graphs comparing PO and MoM RCS are provided in Fig. 2. From Fig. 2, it is evident that as frequency increases, results from PO converge satisfyingly to results of MoM for most of the observation range. As stated previously, PO does not account for the fields diffracted by edges. Considering azimuth graphs in Fig. 2, especially in 600 MHz, it is seen that PO RCS deviates dramatically from MoM results for observation angles corresponding to the front and tail of the vessel. This is due to the fact that the excitation wave is incident on edges located in these positions. Obviously, this error is negligible in high frequencies. This error consumption rises from the fact that the dimensions of the structure are increasing electrically and partitions of the structure approach PO approximation validity region. Therefore, PO requirements are partially fulfilled.

Recalling the fact that PO approximation is valid only for a large target with a smooth surface, it is seen that the convergence in azimuth graphs reaches to a maximum for side views ($\varphi = \pi/2$ and $3\pi/2$). This is due to the fact that the excitation field is mainly incident upon the side walls of the vessel, which can be interpreted as infinite planes in higher frequencies. Also, as seen in Fig. 2, the complexity of RCS rises as frequency increases due to the increase in the resolution of the transceiver.

Tables 2-4 provide the mean and standard deviation of RCS error, devoting a chance of quantitative assessment of PO functionality. In addition, the dimensions of the vessel in terms of

the simulation wavelength and the RCS average value have been shown. As seen in Table 2, the RCS average is approximately 5 dBsm more than RCS error for a minimum D/λ of 1. Considering the azimuth view, the main contribution to RCS is due to the vessel sidewalls, which results in precise PO RCS due to its large dimensions. Therefore, explaining the low error average. Also, for elevation along the width view, the difference between RCS average and RCS error is distinguishable. In this case PO rays are incident upon the central section of the structure, which its cross range is mainly a smooth PEC surface. Therefore, RCS is precisely computed for this view too. This can be also inferred from graphs of Fig. 2 in high frequencies. For elevation along the length however, the error is considerable compared to the RCS average itself. While MoM accounts for the effect of the scatterers set on the infrastructure of the vessel, PO requirements are not met because these scatterers are generally small compared to the wavelength; and although several reflectors are mounted on the main structure, they are not detected by the transceiver resolution cell during PO simulation. This effect is crystal clear in Fig. 2 for 1, 3 and 5 GHz, where the objects on the vessel contribute to MoM backscattered fields, which results in higher RCS values compared to PO backscattering, which possesses low RCS for central values of θ .

In order to grasp a deeper knowledge about the error values in the range of PO reliability, we will

consider the data provided in Table 2 for the central frequency (5 GHz). Assume the vessel is an object with an isotropic RCS pattern with RCS average value. This object has an RCS value of 0.04 square-meters and an RCS toleration value of 0.008 square-meters. Therefore, it is concluded that the detected cross section may oscillate between 0.032 and 0.048 square-meters, which implies the fact that this amount of error may not cause complications from a target detection standpoint. The standard deviation in this region however, occupies a considerable interval, which means the error values are quite extensive in range. In other words, while RCS error is high for specific observations, it is negligible in other view angles in each single frequency.

Although, mean and standard deviation are the main parameters used for analyzing the distribution of a variable, in order to better analyze PO and MoM datasets, the Pearson Product-Moment Correlation Coefficient (PPMCC) defined in equation (13) has been used:

$$r = \frac{\sum_m \sum_n (A_{mn} - \bar{A})(B_{mn} - \bar{B})}{\sqrt{(\sum_m \sum_n (A_{mn} - \bar{A})^2)(\sum_m \sum_n (B_{mn} - \bar{B})^2)}}. \quad (13)$$

This criterion is a measure of the linear correlation between two variables A and B , where \bar{A} and \bar{B} are their mean values, respectively. r is limited to $[-1, 1]$, where 1 implies total positive correlation, 0 implies no correlation and -1 represents total negative correlation.

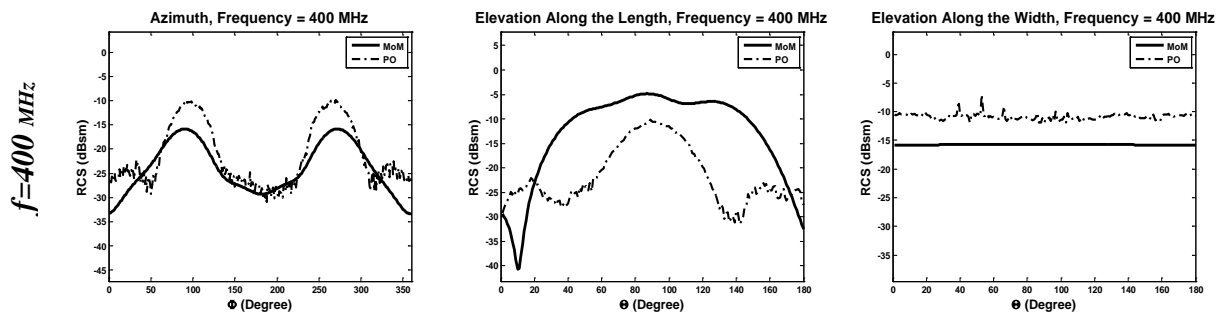


Fig. 2. Comparison of RCS obtained by MoM and PO (dashed marker). Columns represent view aspects azimuth, elevation along the length and elevation along the width.

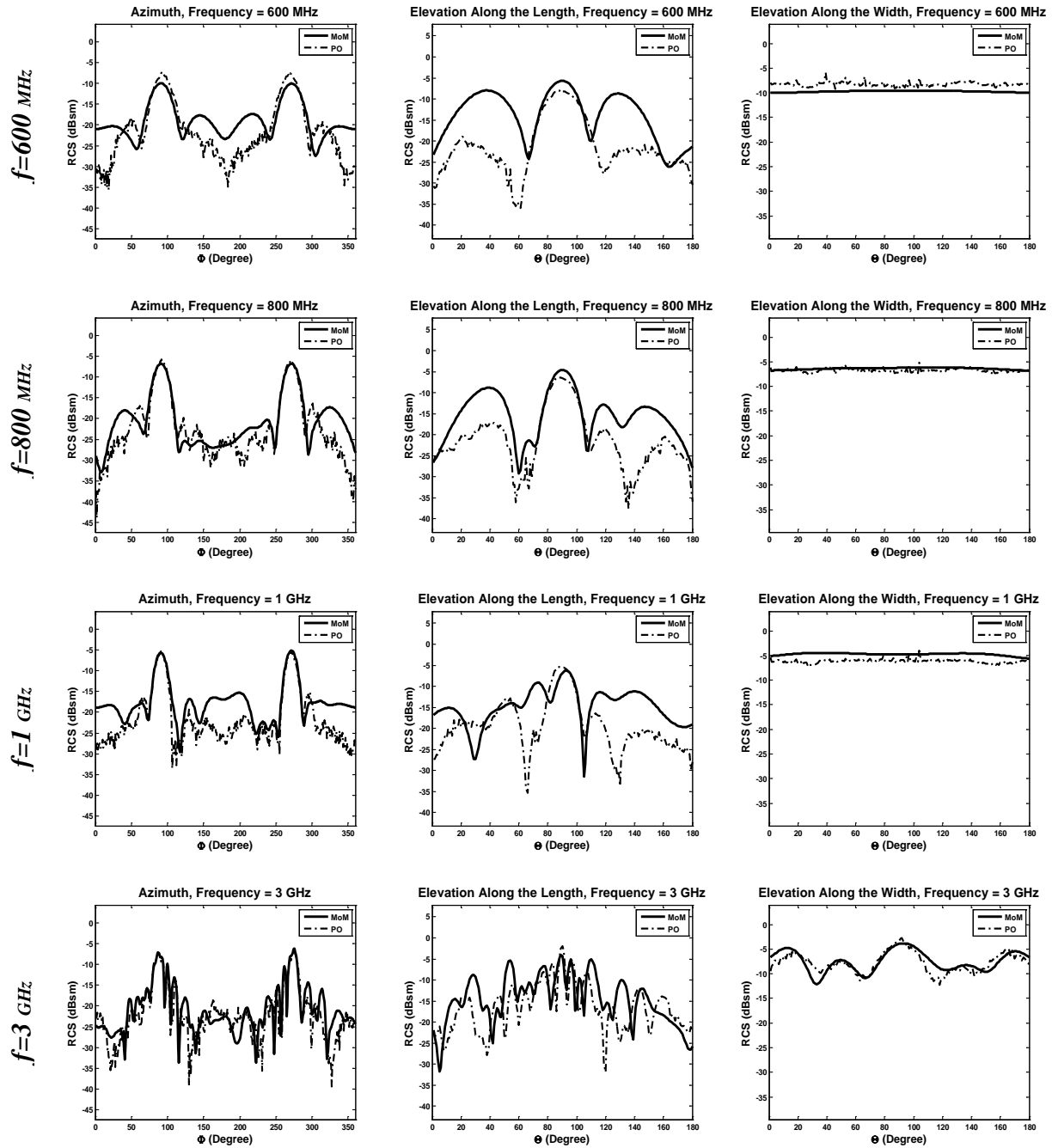


Fig. 2-continued. Comparison of RCS obtained by MoM and PO (dashed marker). Columns represent view aspects azimuth, elevation along the length and elevation along the width. Rows represent each simulation frequency.

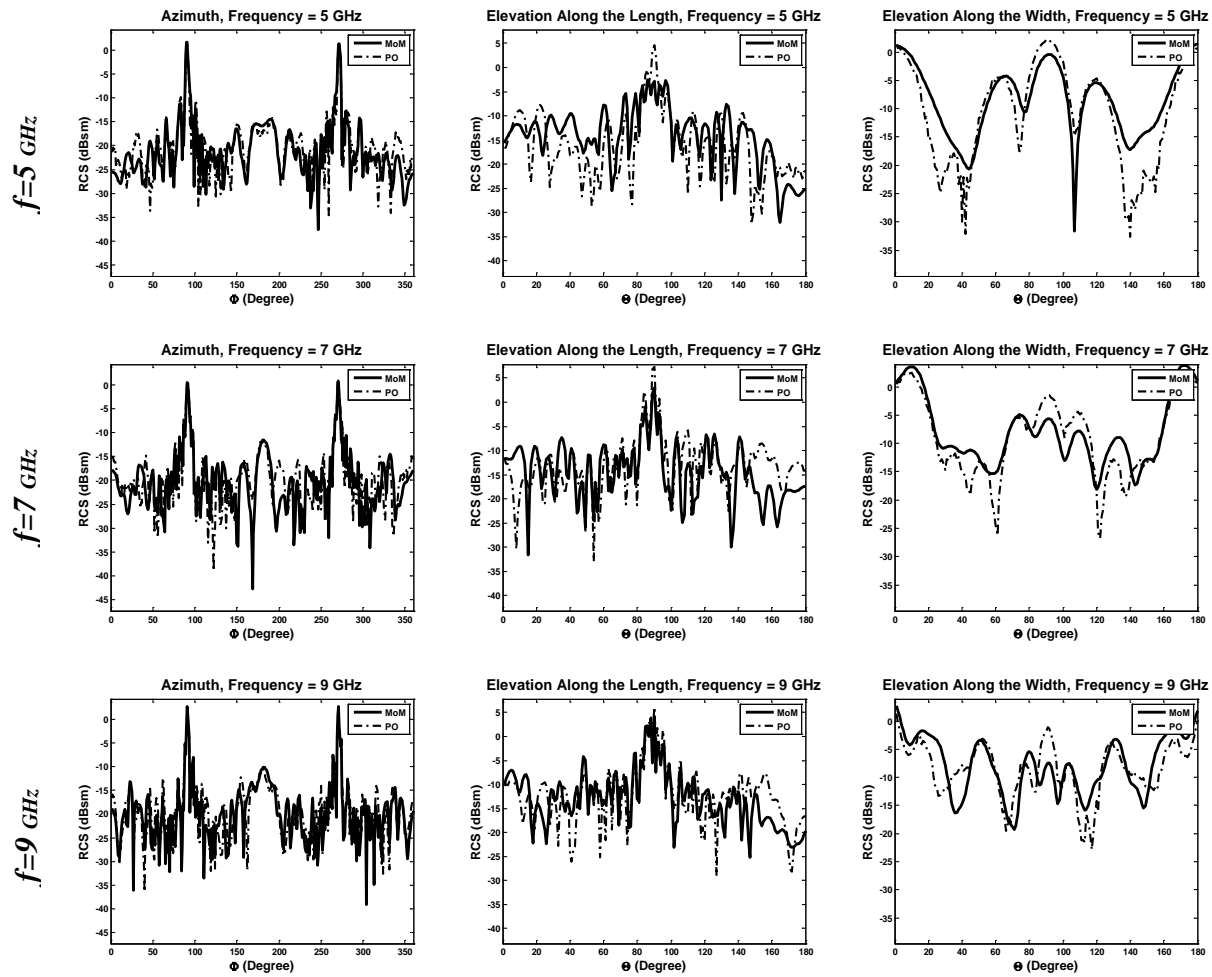


Fig. 2-continued. Comparison of RCS obtained by MoM and PO (dashed marker). Columns represent view aspects azimuth, elevation along the length and elevation along the width. Rows represent each simulation frequency.

Table 2: Error table for azimuth view

Frequency (GHz)	0.4	0.6	0.8	1	3	5	7	9
Length/ λ	0.78	1.17	1.56	1.95	5.87	9.79	13.7	17.62
Width/ λ	0.11	0.16	0.22	0.27	0.82	1.37	1.92	2.47
Height/ λ	0.08	0.12	0.16	0.2	0.62	1.04	1.46	1.88
RCS Avg. (dBsm)	-21.07	-16.62	-15.46	-14.35	-16.65	-14.27	-14.55	-13.74
Error Avg. (dBsm)	-18.4	-18.98	-21.68	-19.4	-22.16	-20.79	-19.49	-18.02
Error Std. (dBsm)	-16.56	-18.16	-21.02	-20.21	-21.16	-17.52	-16.66	-12.96

Table 3: Error table for elevation along the length view

Frequency (GHz)	0.4	0.6	0.8	1	3	5	7	9
Length/ λ	0.78	1.17	1.56	1.95	5.87	9.79	13.7	17.62
Width/ λ	0.11	0.16	0.22	0.27	0.82	1.37	1.92	2.47
Height/ λ	0.08	0.12	0.16	0.2	0.62	1.04	1.46	1.88
RCS Avg. (dBsm)	-8.65	-11.06	-12.08	-12.97	-11.51	-10.81	-10.46	-8.64
Error Avg. (dBsm)	-9.26	-12.57	-14.6	-14.74	-13.06	-10.64	-10.01	-10.74
Error Std. (dBsm)	-10.55	-13	-14.52	-14.75	-12.17	-5.9	-4.27	-7.52

Table 4: Error table for elevation along the width view

Frequency (GHz)	0.4	0.6	0.8	1	3	5	7	9
Length/ λ	0.78	1.17	1.56	1.95	5.87	9.79	13.7	17.62
Width/ λ	0.11	0.16	0.22	0.27	0.82	1.37	1.92	2.47
Height/ λ	0.08	0.12	0.16	0.2	0.62	1.04	1.46	1.88
RCS Avg. (dBsm)	-15.76	-9.73	-6.37	-4.73	-6.97	-5.01	-3.51	-5.33
Error Avg. (dBsm)	-12.49	-13.58	-16.74	-10.26	-13.79	-8.690	-8.260	-8.29
Error Std. (dBsm)	-18.85	-17.76	-18.16	-15.71	-15.03	-7.79	-7.03	-8.37

The PPMCC computed for MoM and PO RCS has been plotted in Fig. 3. High values of r imply the fact that let alone the error, PO RCS has followed the pattern and complexities of precise MoM results. For instance, in Fig. 3 (a), correlation values are close to its maximum. As depicted in Fig. 2 for azimuth view, PO results represent the main features of RCS computed by MoM. Applying the same analysis to Fig. 3 (b), the minimum of correlation occurs in the vicinity of 4 GHz.

Analyzing this based on graphs provided in Fig. 2, it is seen that this interpretation is in good agreement with RCS plots for 1, 3 and 5 GHz, explained previously via error tables. As for elevation along the width view, it is inferred from Fig. 3 (c) that the correlation coefficient is generally less than the azimuth case. Still, high correlation is seen for most of the bandwidth. The same result is concluded from Fig. 2, where PO RCS follows the main aspects of MoM RCS.

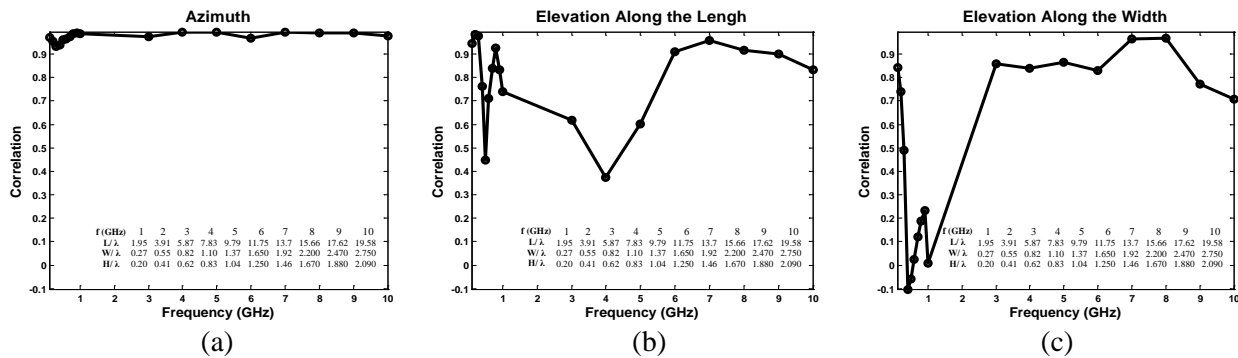


Fig. 3. Correlation graphs between MoM and PO for: (a) azimuth, (b) elevation along the length and (c) elevation along the width. D/λ value regarding each frequency are also provided in the tables.

V. RCS MEASUREMENT

In previous sections, it has been concluded that PO is an expedient replacement for MoM. Confirmation of results provided by PO via measurement will be the final validation for this analysis. Figure 4 shows the designed complex structure in a tapered anechoic chamber located on a pylon of 1 m height. A Continuous Wave (CW) measurement scenario has been carried out, employing the X band standard horn antenna with vertical polarization. RCS measurement has been accomplished at 8.5 GHz for azimuth view in 438 points. The structure is in the far-field of the transceiver with 3 m distance.

Comparison of measurement data with MoM and PO RCS is presented in Figs. 5 and 6, respectively. Also, the average of measured RCS along with the mean and standard deviation of MoM and PO computed RCS are provided in Tables 5-6. As seen in these tables, the average error is close to the RCS mean value itself. However, it should be noted that although the error mean and standard deviation are from the same order of the RCS average, considering the dimensions of the vessel, this error is not misleading as long as detection purposes are of concern. Also, it is seen that measured RCS values are in partial agreement with data provided in Table 2.

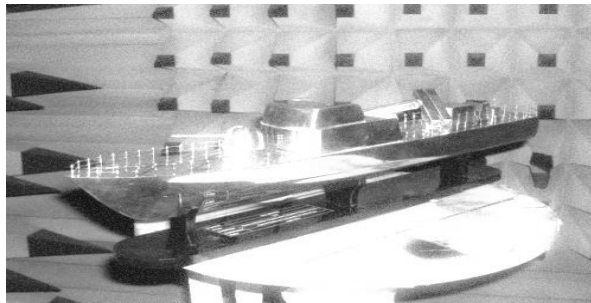


Fig. 4. Designed vessel in anechoic chamber.

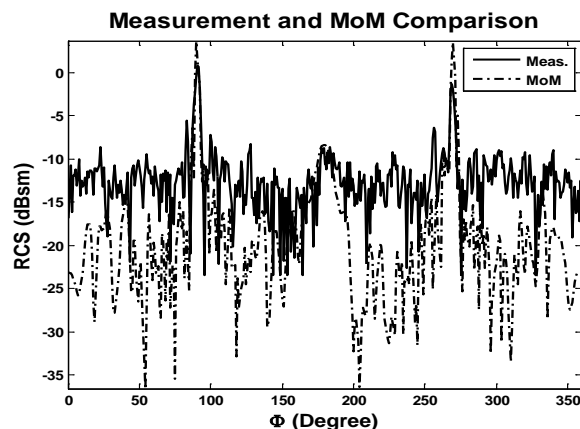


Fig. 5. Comparison of measured and MoM-computed RCS at 8.5 GHz.

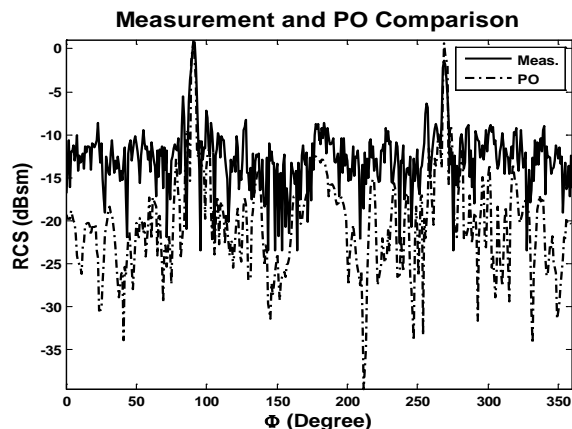


Fig. 6. Comparison of measured and PO-computed RCS at 8.5 GHz.

Table 5: Comparison of measured and MoM-computed RCS

RCS Avg. (dBsm)	Error Avg. (dBsm)	Error Std. (dBsm)
-11.13	-11.99	-8.79

Table 6: Comparison of measured and PO-computed RCS

RCS Avg. (dBsm)	Error Avg. (dBsm)	Error Std. (dBsm)
-11.13	-12.66	-12.38

VI. CONCLUSION

Due to complexities of MoM, PO has been used for RCS prediction of the vessel studied through this paper. On account of this, it has been demonstrated that PO results are invaluable tolerating the cost of temporal erroneous outcomes. Although as defined, PO best suits for EM problems of electrically large structures, it has shown credible for large values of $D\lambda$ during this work. Convergence of results obtained by PO and MoM are acceptable as the minimum $D\lambda$ exceeds 1. Although, error values may seem in considerable comparison with the structures' RCS itself, it should be noted that the impact of this error from target detection standpoint is negligible as the RCS of the structure is not considerable itself. On the other hand, it should be bolded that while the dimensions of complex structures increase, they actually meet PO approximation for high frequency analysis; which consequently results in RCS error reduction.

Error tables provided in this work can serve as a benchmark for quality assessment of future studies involving the development of enhanced high-frequency methods. Studies on the reliability of RCS prediction of maritime targets can be continued, while accounting for the effect of multiple scattering caused by the sea rough surface.

REFERENCES

- [1] R. Firoozabadi, E. L. Miller, C. M. Rappaport, and A. W. Morgenthaler, "Subsurface sensing of buried objects under a randomly rough surface using scattered electromagnetic field data," *IEEE Trans. Geosci. Remote Sens.*, vol. 45, no. 1, pp. 104-117, January 2007.
- [2] G. Wang, Y. Zhang, and M. Amin, "New approach for target locations in the presence of wall ambiguities," *IEEE Trans. Aerosp. Electron. Syst.*, vol. 42, no. 1, pp. 301-315, January 2006.
- [3] Y. S. Yoon and M. G. Amin, "High-resolution through-the-wall radar imaging using beamspace MUSIC," *IEEE Trans. Antennas Propag.*, vol. 56, no. 6, pp. 1763-1774, June 2008.
- [4] P. C. Chang, R. J. Burkholder, J. L. Volakis, R. J. Marhefka, and Y. Bayram, "High-frequency EM

- characterization of through-wall building imaging," *IEEE Trans. Geosci. Remote Sens.*, vol. 47, no. 5, pp. 1375-1387, May 2009.
- [5] T. K. Chan, Y. Kuga, and A. Ishimaru, "Experimental studies on circular SAR imaging in clutter using angular correlation function technique," *IEEE Trans. Geosci. Remote Sens.*, vol. 37, no. 5, pp. 2192-2197, September 1999.
- [6] S. Kidera, T. Sakamoto, and T. Sato, "High-resolution and real-time UWB radar imaging algorithm with direct waveform compensations," *IEEE Trans. Geosci. Remote Sens.*, vol. 46, no. 11, pp. 3503-3513, November 2008.
- [7] L. Du, Y. Wang, W. Hong, W. Tan, and Y. Wu, "A three-dimensional range migration algorithm for downward-looking 3D-SAR with single transmitting and multiple-receiving linear array antennas," *EURASIP J. Adv. Signal Process.*, vol. 2010, article ID 957916, pp. 15, 2010.
- [8] B. R. Mahafza and M. Sajjadi, "Three-dimensional SAR imaging using linear array in transverse motion," *IEEE Trans. Aerosp. Electron. Syst.*, vol. 32, no. 1, pp. 499-510, January 1996.
- [9] S. Jun, X. L. Zhang, J. Y. Yang, and W. Chen, "APC trajectory design for one-active linear-array three-dimensional imaging SAR," *IEEE Trans. Geosci. Remote Sens.*, vol. 48, no. 3, pp. 1470-1486, March 2010.
- [10] W. Matthias and G. Markus, "Initial ARTINO radar experiments," *presented at the 8th European Conference on Synthetic Aperture Radar*, Aachen, Germany, June 2010.
- [11] J. M. Lopez-Sahcnez and J. Fortuny-Guash, "3D radar imaging using range migration techniques," *IEEE Trans. Antennas Propag.*, vol. 48, no. 5, pp. 728-737, May 2000.
- [12] J. Fortuny-Guash and J. M. Lopez-Sahcnez, "Extension of the 3-D range migration algorithm to cylindrical and spherical scanning geometries," *IEEE Trans. Antennas Propag.*, vol. 49, no. 10, pp. 1434-1444, October 2001.
- [13] X. J. Xu and R. M. Narayanan, "Three-dimensional interferometric ISAR imaging for target scattering diagnosis and modeling," *IEEE Trans. Image Process.*, vol. 10, no. 7, pp. 1094-1102, July 2001.
- [14] Budillon, A. Evangelista, and G. Schirinzi, "Three-dimensional SAR focusing from multipass signals using compressive sampling," *IEEE Trans. Geosci. Remote Sens.*, vol. 49, no. 1, pp. 488-499, January 2011.
- [15] W. Qi, M. Xing, G. Lu, and Z. Bao, "High-resolution three-dimensional radar imaging for rapidly spinning targets," *IEEE Trans. Geosci. Remote Sens.*, vol. 46, no. 1, pp. 22-30, January 2008.
- [16] G. Fornaro, D. Reale, and F. Serafino, "Four-dimensional SAR imaging for height estimation and monitoring of single and double scatterers," *IEEE Trans. Geosci. Remote Sens.*, vol. 47, no. 1, pp. 224-237, January 2009.
- [17] S. Kidera, T. Sakamoto, and T. Sato, "High-resolution 3-D imaging algorithm with an envelope of modified spheres for UWB through-the-wall radars," *IEEE Trans. Antennas Propag.*, vol. 57, no. 11, pp. 3520-3529, November 2009.
- [18] Y. Zhang, D. Huang, and J. Chen, "Combination of asymptotic phase basis functions and matrix interpolation method for fast analysis of monostatic RCS," *Applied Computational Electromagnetics Society (ACES) Journal*, vol. 28, no. 1, pp. 49-56, January 2013.
- [19] Z. Liu, R. Chen, J. Chen, and Z. Fan, "Using adaptive cross approximation for efficient calculation of monostatic scattering with multiple incident angles," *Applied Computational Electromagnetics Society (ACES) Journal*, vol. 26, no. 4, pp. 325-333, April 2011.
- [20] A. R. Mallahzadeh, J. Rashed-Mohassel, and M. Soleimani, "RCS computation of targets using three dimensional scalar parabolic equation," *Applied Computational Electromagnetics Society (ACES) Journal*, vol. 22, no. 2, pp. 254-259, July 2007.
- [21] G. A. Deschamps, "Ray techniques in electromagnetics," *Proc. IEEE*, vol. 60, no. 9, pp. 1022-1035, September 1972.
- [22] J. B. Keller, "Geometrical theory of diffraction," *J. Opt. Soc. Amer.*, vol. 52, pp. 116-119, February 1962.
- [23] P. Y. Ufimtsev, "Method of edge waves in the physical theory of diffraction," (in Russian) *Transl.:Metod krayevykh volnv fizicheskoy teorii difraktsiiIzd-Vo Sov, Radio*, pp. 1-243, 1962.
- [24] R. Solimene, A. Buonanno, F. Soldovieri, and R. Pierri, "Physical optics imaging of 3-D PEC objects: vector and multipolarized approaches," *IEEE Trans. Geosci. Remote Sens.*, vol. 48, no. 4, pp. 1799-1808, April 2010.
- [25] S. L. H. Ling and R. Chou, "Shooting and bouncing rays: calculating the RCS of an arbitrarily shaped cavity," *IEEE Trans. Antennas Propagat.*, vol. 37, pp. 194-205, February 1989.
- [26] H. Biglary and M. Dehmollaian, "Scattering of an object above a rough surface with impedance boundaries using IPO and FMM," *presented at IEEE Antennas and Propagation Society International Symposium*, Chicago, IL, July 8-14, 2012.
- [27] H. Biglary and M. Dehmollaian, "RCS of a target above a random rough surface with impedance boundaries using GO and PO methods," *presented*

at *IEEE Antennas and Propagation Society International Symposium*, Chicago, IL, July 8-14, 2012.

- [28] A. Ishimaru, "Electromagnetic wave propagation, radiation and scattering," 1st ed., *Englewood Cliffs, NJ: Prentice-Hall*, 1991.
- [29] N. T. Nguyen, A. Rolland, and R. Sauleau, "Range of validity and accuracy of the hybrid GO-PO method for the analysis of reduced-size lens antennas: benchmarking with BoR-FDTD," presented at *Asia-Pacific Microwave Conference*, Macau, December 16-20, 2008.
- [30] T. F. Eibert, "Modeling and design of offset parabolic reflector antennas using physical optics and multilevel fast multipole method accelerated method of moments," presented at *IEEE Multitopic Conference*, Islamabad, December 23-24, 2006.
- [31] J. Perez and M. F. Catedra, "Application of physical optics to the RCS computation of bodies modeled with NURBS surfaces," *IEEE Trans. Antennas Propag.*, vol. 42, pp. 1404-1411, October 1994.
- [32] www.cst.com
- [33] R. Bhalla and Hao Ling "A fast algorithm for signature prediction and image formation using the shooting and bouncing ray technique," *IEEE Trans. Antennas Propag.*, vol. 43, pp. 727-731, July 1995.
- [34] I. Y. Kelly, G. Benavides, R. Bhalla, H. Ling, W. J. Vogel, and H. D. Foltz, "Urban channel propagation modeling using the shooting and bouncing ray technique," presented at *IEEE Antennas and Propagation Society International Symposium*, Montreal, Quebec, Canada, July 13-18, 1997.



Amin B. Gorji was born in Cardiff, UK, in 1989. He received his B.Sc. degree in Electrical Engineering from Babol Noshirvani University of Technology, Babol, Iran in 2011. He is currently advancing his M.Sc. degree in Electromagnetics Engineering at Babol Noshirvani University of Technology. Since 2011, he has been an Assistant and Researcher with the Antenna and Microwave Laboratory, Babol Noshirvani University of Technology. His scientific fields of interest include microwave imaging based on time-reversal methods, measurement techniques of radar cross section and EM numerical techniques for solving scattering and radiation problems.



Bijan Zakeri was born in Babol, Iran in 1974. He received his M.Sc. and Ph.D. degrees in Electromagnetics Engineering from Amirkabir "Polytechnic" University of Technology, Tehran, Iran in 1999 and 2007, respectively. Since 2010, he is an Assistant Professor with Babol Noshirvani University of Technology, Babol, Iran. He also is the Director of Antenna and Microwave Laboratory and the Head of the Radar Research Team at Babol Noshirvani University of Technology. In 2011, he became the Head of the joint research project of Iran Marine Industries Organization (MIO) and Babol Noshirvani University of Technology entitled "*RCS, IR, and Acoustic Signature Reduction of Surface Naval Ships*." He is currently a member of the Iranian Association of Information and Communication Technology. His current research activities are in the fields of computational electromagnetics, inverse scattering, radar microwave subsystems design, UWB antenna and Polin-SAR remote sensing.



Reza C. Janalizadeh was born in Rorkee, India in 1990. Since 2009, he has been preceding his B.Sc. undergraduate studies in Electrical Engineering at the University of Tehran, Tehran, Iran. In 2012, he joined the Antenna and Microwave Laboratory, Babol Noshirvani University of Technology, Babol, Iran as a Researcher in electromagnetic scattering field areas. His research interests include microwave radar remote sensing, EM scattering and wave propagation, inverse scattering and computational electromagnetics.